Acta Geotechnica (2019) 14:1871–1881
https://doi.org/10.1007/s11440-019-00834-6

RESEARCH PAPER

Stress–dilatancy relationship for fiber-reinforced sand and its modeling

Yuxia Kong[1] · Annan Zhou[2] · Feifan Shen[1] · Yangping Yao[3]

Received: 19 April 2018 / Accepted: 3 June 2019 / Published online: 5 October 2019

Abstract
The stress–dilatancy relationship could be employed as the foundation to develop a constitutive model for polypropylene fiber-reinforced (PFR) soils. In this study, a number of triaxial compression tests were carried out to investigate the effect of uniform distributed fiber reinforcements on the stress dilatancy relationship of Nanjing sand. A new parameter representing the increase in the effective confining stress σ_{FR} was introduced to describe the stress–dilatancy of PFR sand, and a new stress–dilatancy relationship was proposed for PFR sand based on Rowe's stress–dilatancy equation for granular materials. Moreover, the stress–dilatancy relationships in the conventional triaxial compression, extension and plane stain conditions were discussed in this paper. The stress–dilatancy relationship is validated against a series of triaxial tests on Nanjing sand and Hostun RF sand mixed with discrete polypropylene fibers. It is shown that the predicted results are in a good agreement with the experimental results.

Keywords Fiber reinforcement · Sand · Stress dilatancy · Triaxial testing

1 Introduction

Earth reinforcement is an effective and reliable technique to increase the strength and stability of soils. The treatment of granular soils with discrete short fiber inclusions can increase soil strength while also affecting the deformation characteristics of the material. Soil reinforcement due to the inclusion of fiber can be attributed to a few factors. Among them, the extension of fibers owing to rearrangement and microstructure disturbance during shearing provides an important contribution to the strength augment. For example, Tang et al. [22] studied the micromechanical interaction behavior between soil particles and fiber by using scanning electron microscopy (SEM). Their study shows that, during shear process, randomly distributed polypropylene fibers are mobilized against tension and this provides an important component in soil reinforcement. The use of random discrete flexible fibers mimics the behavior of plant roots and gives the possibility of improving the strength and the stability of near surface soil layers [4, 24]. Fiber reinforcement presents a promising alternative in the projects involving ether localized repair of slopes or reinforcement of thin soil veneers, especially when the planar reinforcement (e.g., with geotextiles and geogrids) is difficult to implement. Over the last decades, geotechnical engineers have been employing this technique for the stabilization of thin layers of soil, repairing failed slopes, liquefaction resistance, soil strengthening around footings and earth retaining structures [14, 15, 17].

A large number of experiments have been conducted to investigate the mechanical behavior of flexible fiber-reinforced soils [2, 3, 5, 7, 14]. The experimental results show

✉ Yuxia Kong
kongyuxia@njtech.edu.cn

Annan Zhou
annan.zhou@rmit.edu.au

Feifan Shen
shenfeifanhn@163.com

Yangping Yao
ypyao@buaa.edu.cn

[1] Institute of Geotechnical Engineering, Nanjing Tech University, NO.30 Puzhu Road(S), Nanjing 211800, Jiangsu, China

[2] School of Engineering, Royal Melbourne Institute of Technology, Melbourne, VIC 3001, Australia

[3] Department of Civil Engineering, Beihang University, No. 37 Xueyuan Road, Beijing, China

that the efficiency of fiber treatment is highly dependent on the fiber concentration, soil matrix physical characteristics and their spatial configuration. The sand fiber composites were found to have bilinear failure envelopes for the peak strength, with the breakage occurring at a threshold confining stress named critical confining stress [2, 14]. In a discrete framework proposed by Zornberg [25], fibers increase the shear strength by enlarging the tensile strength. It was found that the bond strength and friction at the interface are controlling the effectiveness of reinforcement. Bond strength is the strength of interfacial bonds between fiber and enwrapped soil particles. Interface friction means the friction between soil particles and fiber [22]. The insertion of fibers randomly into the sand changes not only its shearing behavior but also its isotropic compression behavior [7]. A description of the local fiber soil stress transfer mechanism for fiber-reinforced granular soils based on a modified shear lag theory had been presented by Diambra and Ibraim [3]. Unlike the pure sand, the compressive part of the stress–dilatancy does not depend on stress level, with approach paths forming a narrow band [19]. Dos Santos et al. [20] examined the behavior of fiber-reinforced soils in terms of the critical state soil mechanics framework, reporting slightly different trends for the reinforcement effect between low to medium and high stresses. Madhusudhan et al. [13] have found that the normal compression line and critical state line of the reinforced soil are parallel and above those of the unreinforced soil. Li et al. [12] reported on the behavior of a carbon fiber-reinforced granular soil, and a unique relationship was observed between peak strength and the state parameter, which was found to be independent of the fiber content.

The dilatancy effect was first described scientifically by Reynolds at 1885 [16], and long afterward, Rowe introduced a stress–dilatancy theory for an assembly of particles in contact, which stated that, for a sand sample that is being sheared, the ratio of the work done by the driving stress to the work done by the driven stress in any strain increment should be a constant [18].

Stress–dilatancy relationship plays an essential role in constitutive modeling for soils [1, 9, 10, 23]. The concept of fiber space was introduced by Wood et al. to describe the significant changes in dilatancy of fiber-reinforced sand [24]. However, there is a knowledge gap between the existing understanding of the fiber-reinforced sand and the observed stress dilatancy of the fiber-reinforced sand. When a polypropylene fiber soil assembly dilates in response to the applied shear deformations, the work done by the driving stress will be dissipated by not only the particle rearrangement but also the fiber deformation.

To investigate the stress–dilatancy behavior of sand mixed with flexible polypropylene fibers, 20 drained triaxial compression tests were conducted in this research. The laboratory observations presented here focused on the stress–dilatancy behavior of sand mixed with flexible polypropylene fibers. A parameter, representing the effect of fiber on the effective confining stress, σ_{FR} (Fig. 1), was introduced to describe the stress–dilatancy of fiber-reinforced sand, and the work dissipated by the polypropylene fiber sand deformation was expressed in detail in this study. Based on the minimum rate of internal work assumption, the stress–dilatancy relationship is proposed to consider both the particle sliding and the fiber deformation. The proposed stress–dilatancy relationships with conventional triaxial compression, extension and plane stain conditions were discussed and analyzed.

2 Experimental testing program

2.1 Material tested

The material tested in this study was made of Nanjing sand and discrete polypropylene fibers. Nanjing sand was sampled from the beach of Yangtze River in the region of Nanjing, China. It can be described as a fine, clean quartzitic sand with a uniform grading (Fig. 2). The characteristics of Nanjing sand are given in Table 1. The specific gravity of the solid grain is 2.69. The mineralogical analysis showed that sand particles are predominantly quartz. The minimum and maximum void ratios are 0.80 and 1.24, respectively. The fibers used in the laboratory testing program are commercially available polypropylene fibers. Nanjing sand was reinforced with discrete polypropylene fibers with the average dimensions 12 mm in length, 0.0015 mm in diameter, and with specific density of 0.91, tensile strength of 460 MPa and elastic modulus of 3.5 MPa. The fiber content, χ_w, used in the experiments was 0.15, 0.25, 0.35 and 0.5% by weight of sand.

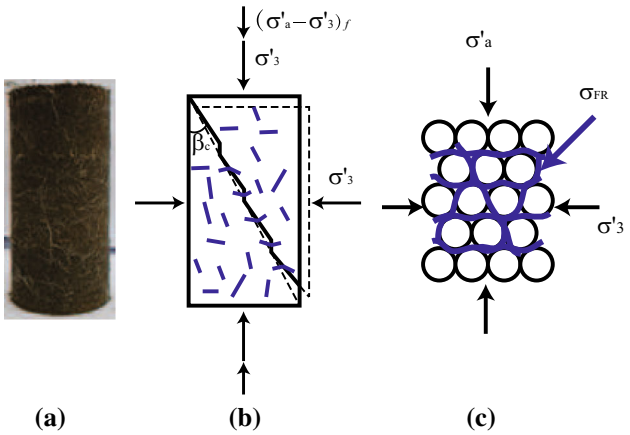

Fig. 1 Bridge effect of fiber reinforcement

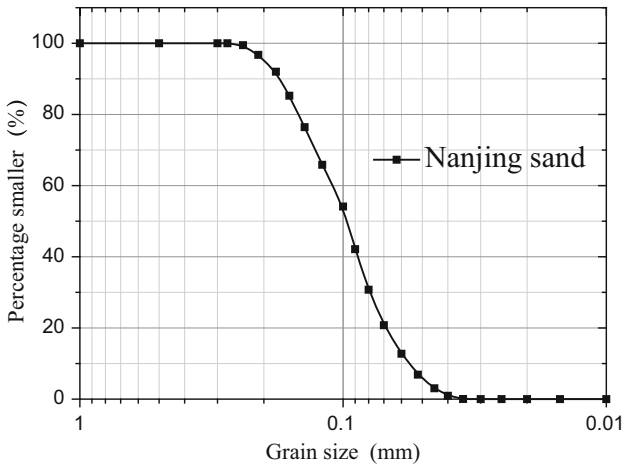

Fig. 2 Grain size diagram

Table 1 Properties of Nanjing sand

Properties	Nanjing sand
Specific gravity of solids	2.69
Uniformity coefficient, C_u	2
Curvature coefficient, C_c	1.06
Effective diameter, D_{10} : mm	0.055
Effective diameter, D_{30} : mm	0.080
Mean diameter, D_{60} : mm	0.11
Minimum void ratio, e_{min}	0.80
Maximum void ratio, e_{max}	1.24

2.2 Testing procedures

The desired fiber amount was determined considering the dry weight of Nanjing sand and the desired gravimetric fiber content when preparing each specimen. The compacted sand and fiber-reinforced specimens for triaxial tests were prepared by hand-mixing dry sand, water and polypropylene fibers. To prevent floating of the fibers, it is important to add the water before adding the fibers during the mixing process. The specimens were statically compacted in three layers into a 39.1 mm diameter by 80 mm high split mold. Visual inspection (Fig. 1a) showed that good uniformity was achieved.

As shown in Table 2, the triaxial tests were carried out on the samples fully saturated using effective confining pressures ranging from 50 to 300 kPa with the GDS Triaxial Automated System (GDSTAS). Firstly, we use vacuum evaporation method and then use back pressure saturation method. The degree of saturation was monitored in each test, ensuring B values of at least 0.95 for all specimens. Axial and radial strains were monitored inside the triaxial cell automatically. Full drainage during the shearing process was ensured using a sufficiently low applied axial strain 0.08 mm/min and was monitored by measuring the excess pore pressure at the opposite end of the specimen to the drainage.

3 Fiber sand behavior during triaxial sharing

3.1 Stress–strain during shearing

Table 2 shows the tests carried out in this study. Specimens of non-reinforced and reinforced sand were isotropically consolidated to pressures of 50 kPa, 100 kPa, 200 kPa and 300 kPa before shearing drained while keeping the cell pressure constant. The ranges of initial fabrication void ratios used for the pure sand and sand fiber specimens were similar, varying between 0.85 and 0.86.

Typical stress–strain data for tests on polypropylene fiber-reinforced samples of Nanjing sand are shown in Fig. 3. Tests results include shear stress and volumetric strain versus axial strain plots for specimens tested at confining stress levels of 50, 100, 200 and 300 kPa. The reinforcing effect in Nanjing sand is more distinct when the stress level is low. With the same stress level, the composite behavior is closely related to the fiber content χ_w. Data presented in Fig. 3 indicate a maximum improvement in shear strength for the fiber content of $\chi_w = 0.35\%$. It indicated that $\chi_w = 0.35\%$ is the best of the four serials of experiment carried out in this research subjected to different fiber contents, and $\chi_w = 0.35\%$ may be the nearest to the optimum fiber content of the four. If the fiber content was lower than the optimal fiber content, fibers can't interlock in the soil. If the fiber content was higher than the

Table 2 Tests carried out in this study

Material	Type of test	Fiber content, χ_w (%)	Confining stress (kPa)
Sand	Triaxial compression	0	50; 100; 200; 300
Sand fiber	Triaxial compression	0.15, 0.25, 0.35, 0.5	50; 100; 200; 300

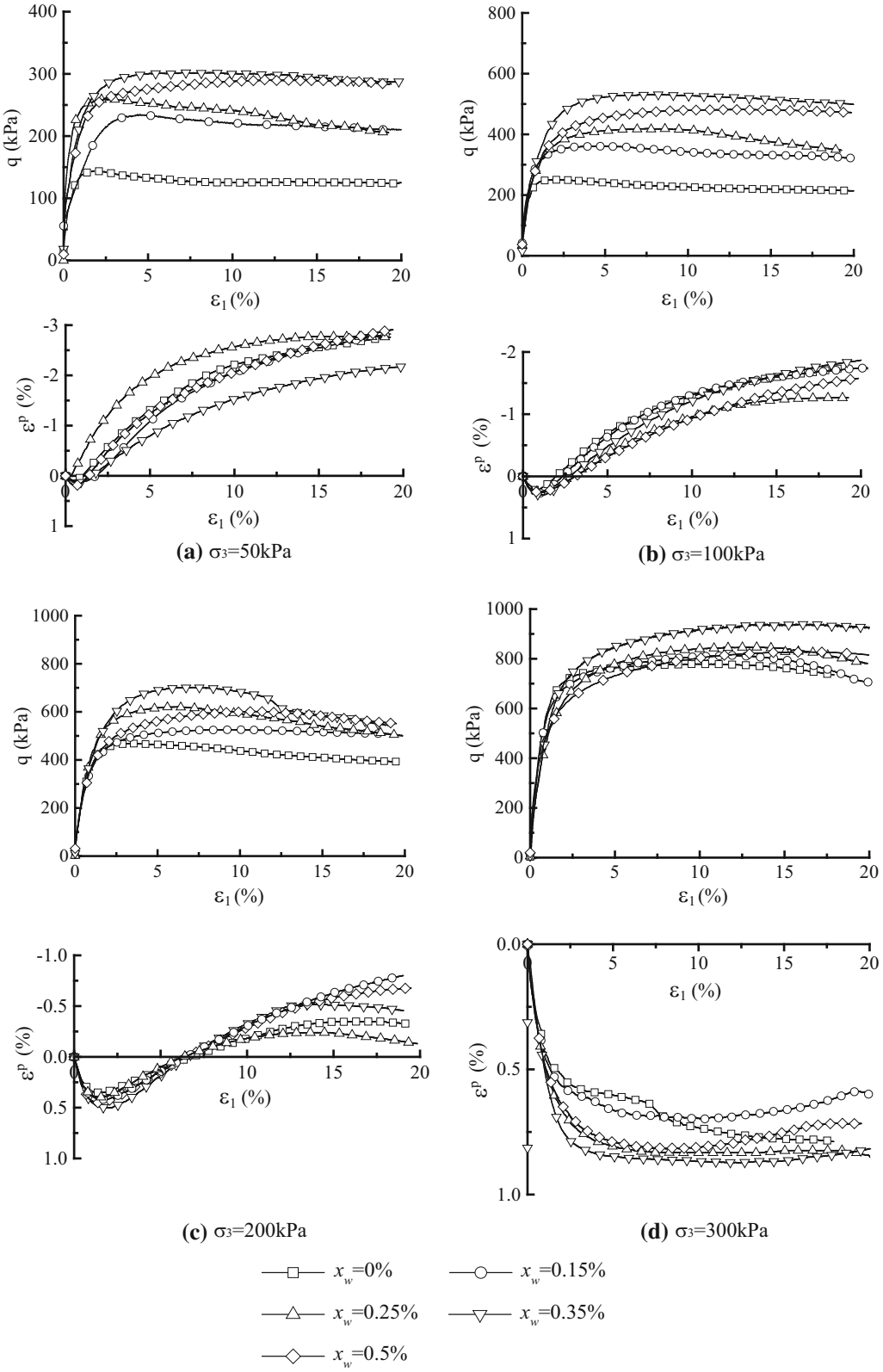

Fig. 3 Stress–strain–volumetric response of Nanjing sand and fiber-reinforced sand for different confining pressures

optimal fiber content, fibers may form weak structural plane in the sand. The volumetric response for both reinforced sand and unenforced sand showed an initial compression and followed by dilation (Fig. 3b, c). The volumetric behavior is clearly affected by the addition of fibers and the confining stresses.

3.2 Shear strength

Figure 4 shows the shear strength envelopes of pure Nanjing sand and fiber-reinforced sand in $q - p'$ plane, with different fiber contents (χ_w). The critical state points for pure sand define a straight line, while bilinear failure envelope for other sand fiber combinations. The deviatoric stresses at the kink point with different fiber contents are shown in Fig. 5. Before the kink point, failure is governed by fiber stretching, slippage and mobilization in the matrix. After the kink point, failure is governed by tensile yielding, stretching of the fiber and mobilization. Strains will develop in the fibers because of the strains that occur in the soil around the fibers. In their interaction with the soil, as the strains increase, the fibers may pullout of the soil or may reach their tensile strength.

Figure 6 shows the friction angle of peak strength against state parameter $(\xi + 1)$ for the unreinforced and reinforced Nanjing sand. As shown in the above figure, the ϕ_{peak}–$(\xi + 1)$ curves converge along with the increase of $(\xi + 1)$. The state $(\xi + 1) > 1$ indicates shear contraction, and the state $(\xi + 1) < 1$ implies shear dilation. Our results show that the effect of fiber content on the peak strength is more distinct when shear dilation predominates, while the effect of fiber content on the peak strength is much less distinct when shear contraction prevails. This observation

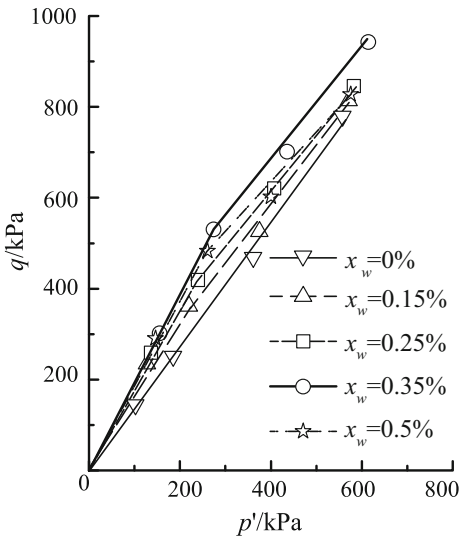

Fig. 4 Shear strength envelopes of Nanjing sand and fiber-reinforced sand in $q - p'$ plane with different fiber contents

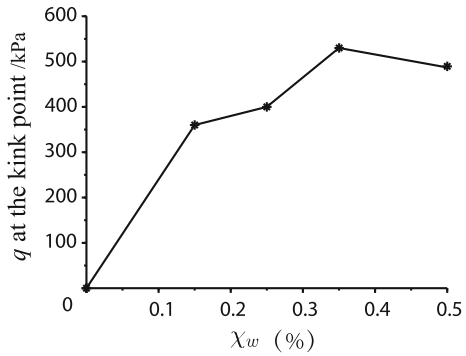

Fig. 5 q at the kink point with different fiber contents χ_w

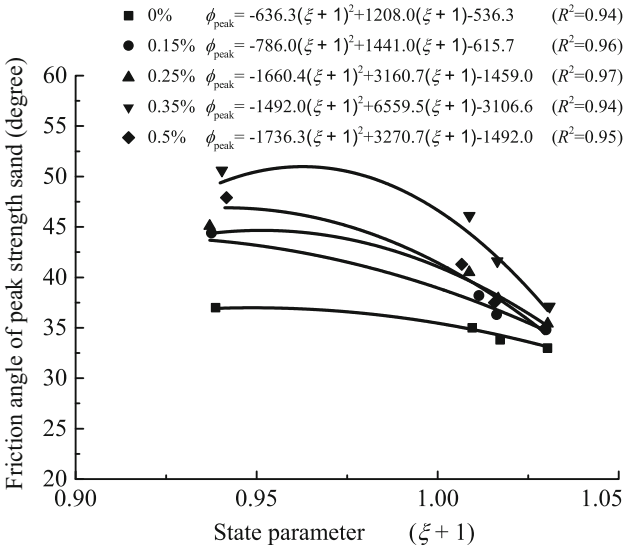

Fig. 6 Friction angle of peak strength, ϕ_{peak}, against state parameter, $(\xi + 1)$, for the unreinforced and reinforced Nanjing sand

is reasonably explained by using the mobilization of soil particles. In the shear dilation, the fibers undergo higher tension due to the departing movement of particles. Therefore, the content of fiber imposes much more influences on the peak strength. On the other hand, for shear contraction, the tension of fibers is relatively weak (some of them may be even undergoing compression) because the particles move toward each other resulting volume reduction. Therefore, the influence of the content of fiber is weak correspondingly.

The fiber we used in this study is almost double length to the fiber used in Li et al. [12]. The deference between the tension and compression for longer fibers is expected to be more distinct compared with that between the short fibers. This could be another reason to explain that Li et al. [12] observed a normalized relationship between ϕ_{peak} and $(\xi + 1)$ while we observed a convergency of different ϕ_{peak}–$(\xi + 1)$ curves along with the increase of $(\xi + 1)$.

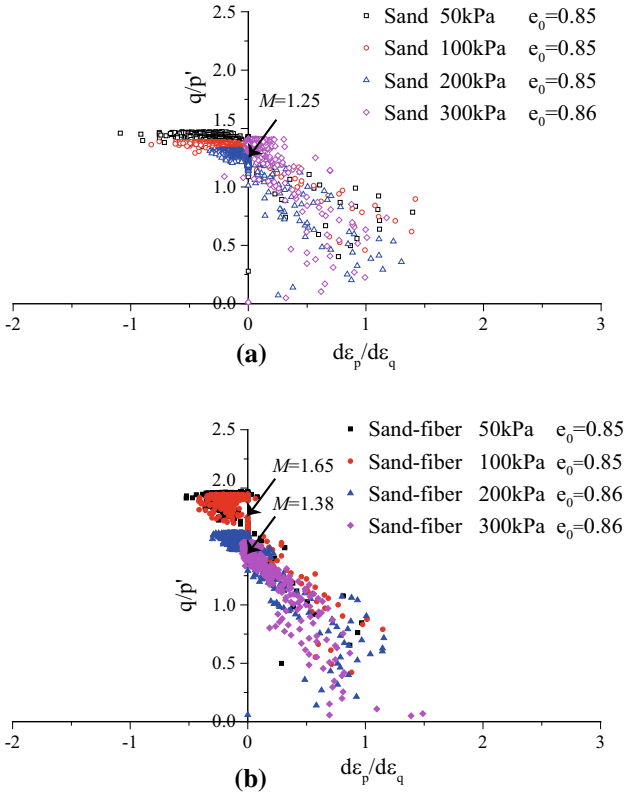

Fig. 7 Stress–dilatancy response of **a** Nanjing sand and **b** fiber-reinforced sand

3.3 Stress–dilatancy

Figure 7 compares the stress–dilatancy behavior of pure sand (see Fig. 7a) and fiber-reinforced sand with 0.35% polypropylene fibers (see Fig. 7b). For pure dense Nanjing sand (Fig. 7a), specimens tested at 50 kPa, 100 kPa, 200 kPa and 300 kPa confining stresses showed that the volumetric strain increments are almost zero at the stress ratio $1.25 < \eta < 1.45$. Figure 7b shows the results for sand fiber material. The confining pressure seems to influence the dilatancy behavior: with confining pressures of 50 kPa and 100 kPa, the compression does not stop at reaching a rate of volumetric change $\delta\varepsilon_p/\delta\varepsilon_q = 0$ at the stress ratio $\eta = M = 1.65$, but is following a clear dilation, which then reaches to a critical state ratio equal to 1.85. Thus, at lower confining stresses the inclusion of fibers increases the critical state ratio. The specimen tested at 200 kPa and 300 kPa confining stresses showed that the volumetric strain increments were zero at the stress ratio $\eta = M = 1.38$ and only a small dilation up to a peak dilation rate.

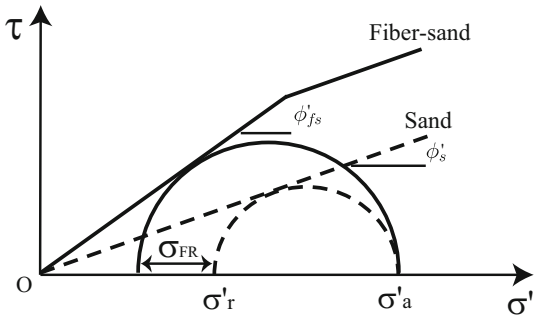

Fig. 8 Reinforcing effect of fiber on the effective confining stress, σ_{FR}, in Mohr circle space

4 Stress–dilatancy relationship for fiber-reinforced sand

4.1 Contributions of fibers

As shown in Fig. 8, bilinear failure envelopes for fiber soils were also reported by Gray and AI-Refeai [6] and Consoli et al. [2]. For the failure occurring below the kink point separating the bilinear failure envelope, there is a composite of slippage and yielding of fibers. For the specimens failing on the higher pressure part of the bilinear failure envelope, there is more distinct fiber stretching. The reinforcing effect of fiber sand results in the mobilization of shear strength in excess of the frictional shear strength of the pure sand [2]. Landva and La Rochelle [11] quantified the reinforcing effect of peat fibers in terms of an additional horizontal reinforcement stress (σ_{FR}) beyond the effective confining stress to ensure that at a given axial effective stress the stress state of the specimen represented by Mohr circle satisfies the Mohr–Coulomb failure criterion corresponding to the frictional shear strength. The shear resistance of fibrous peat over and above the frictional component of the shear strength was assessed in terms of σ_{FR} provided by the tension mobilized by the fibers [8]. This idea can also be adopted to describe the mechanics of fiber-reinforced granular materials, as shown in Fig. 8. σ_{FR} represents the reinforcing effect of fiber on the effective confining stress. ϕ'_s and ϕ'_{fs} are the mobilized friction angles for host soil and fiber-reinforced soil, respectively.

Using simple trigonometry, the effect of fiber on the effective confining stress, σ_{FR}, can be written as

$$\sigma_{FR} = A\sigma'_a = (k_s - k_{fs})\sigma'_a \quad (1)$$

where $k_s = (1 - \sin\phi'_s)/(1 + \sin\phi'_s)$, $k_{fs} = (1 - \sin\phi'_{fs})/(1 + \sin\phi'_{fs})$.

$$A = k_s - k_{fs} \quad (2)$$

The physical manifestation of dilatancy was first identified by Reynolds [16], and long afterward, Rowe [18]

introduced a stress–dilatancy theory for assembly of particles in contact. The relationship between plastic strain increment ratio ($\delta\varepsilon_p^p/\delta\varepsilon_q^p$) and stress ratio ($\eta = q/p'$) is known as a flow rule governing the mechanism of plastic deformation of the soil. The ratio $\delta\varepsilon_p^p/\delta\varepsilon_q^p$ is the plastic dilatancy of the soil, and the resulting plots in terms of the angle β and stress ratio η are called stress–dilatancy diagrams.

$$\tan\beta = \frac{\delta\varepsilon_q^p}{\delta\varepsilon_p^p} \tag{3}$$

Rowes stress–dilatancy relationship for cohesionless materials has been recognized a cornerstone of soil mechanics. Rowe [18] produced an expression which states that, for the soil sample that is being sheared, the ratio of the work done by the driving stress to the work done by the driven stress in any strain increment should be a constant K:

$$\frac{\text{work put in by driving stress}}{\text{work taken out by driven stress}} = -K \tag{4}$$

The constant K is related to the angle of soil friction ϕ_f' by the expression

$$K = \tan^2\left(\frac{\pi}{4} + \frac{\phi_f'}{2}\right) = \frac{1+\sin\phi_f'}{1-\sin\phi_f'} \tag{5}$$

Rowe suggests that the angle ϕ_f' lies in the range of

$$\phi_\mu \le \phi_f' \le \phi_{cs}' \tag{6}$$

where ϕ_{cs}' is the critical state angle of friction for constant volume shearing, and ϕ_μ is the angle of interparticle sliding friction.

The "bridge" effect at the interface between fiber surface and soil matrix was analyzed by Tang et al. [21], using scanning electron microscopy. The "bridge" effect of fiber reinforcement will increase the effective confining stress, and the increment should be considered in the stress–dilatancy relationship. The ratio of the work done by the driving stress to the work done by the driven stress in any strain increment for fiber soils is considered to be different from that of pure sand. The tensile strains in the sand stretch the fibers, and the stretched fibers have a potential resist extension. Therefore, it is noted that σ_{FR} plays a role as driven stress and contributes to the work done on the fiber sand. Using σ_{FR}, the "bridge" effect of fiber reinforcement (Fig. 1c) could be considered in the stress–dilatancy relationship.

4.2 Stress–dilatancy relationship for fiber-reinforced sand under triaxial compression

In conventional triaxial compression (CTC), the axial stress σ_a' is the driving stress (with an associated compressive strain increment $\delta\varepsilon_a$); the radial stresses σ_r' and σ_{FR} are the driven stresses (with an associated tensile strain increment $-\delta\varepsilon_r$). Considering σ_{FR}, the stress–dilatancy relationship for fiber sand for triaxial compression then can be expressed as

$$\frac{\sigma_a'\delta\varepsilon_a}{-2(\sigma_r'+\sigma_{FR})\delta\varepsilon_r} = K_{fs} \tag{7}$$

$$\sigma_a' = p' + \frac{2}{3}q \tag{8}$$

$$\sigma_r' = p' - \frac{1}{3}q \tag{9}$$

$$\varepsilon_p = \varepsilon_a + 2\varepsilon_r \tag{10}$$

$$\varepsilon_q = \frac{2}{3}(\varepsilon_a - \varepsilon_r); \tag{11}$$

here K_{fs} is the extension of K for fiber sand. We use the conventional stress and strain variables for axisymmetric triaxial conditions: p' and q are, respectively, the mean and deviatoric stresses acting on the composite. The stress ratio is $\eta = q/p'$. $\delta\varepsilon_p$ and $\delta\varepsilon_q$ are the volumetric strain and shear strain of the fiber sand.

Using Eqs. 1 and 7, the stress–dilatancy for triaxial compression can be rewritten as follows:

$$\frac{\delta\varepsilon_p}{\delta\varepsilon_q} = \frac{3\eta(K_{fs}+2-2AK_{fs}) - 9(K_{fs}-1-AK_{fs})}{2\eta(K_{fs}-1-2AK_{fs}) - 3(2K_{fs}+1+2AK_{fs})} \tag{12}$$

For fiber sand, it is convenient to fix the value of ϕ_f' at the ultimate critical state value ϕ_{fs}'. Then, the constant K_{fs} becomes

$$K_{fs} = \frac{3+2M_{fs}}{3-M_{fs}} \tag{13}$$

where $M_{fs} = 6\sin\phi_{fs}'/(3-\sin\phi_{fs}')$.

4.3 Stress–dilatancy relationship for fiber-reinforced sand under triaxial extension

For conditions of conventional triaxial extension (CTE), the radial stress σ_r' is the driving stress and the axial stress σ_a' and the effect of fiber on the confining stress σ_{FR} become driven stresses; thus, the stress–dilatancy becomes

$$\frac{2\sigma_r'\delta\varepsilon_r}{-(\sigma_a'+\sigma_{FR})\delta\varepsilon_a} = K_{fs} \tag{14}$$

The equivalent of Eq. 12 for triaxial extension is then

$$\frac{\delta\varepsilon_p}{\delta\varepsilon_q} = \frac{3\eta(2K_{\mathrm{fs}} + 1 + 2AK_{\mathrm{fs}}) + 9(K_{\mathrm{fs}} - 1 + AK_{\mathrm{fs}})}{2\eta(1 - K_{\mathrm{fs}} - AK_{\mathrm{fs}}) - 3(K_{\mathrm{fs}} + 2 + AK_{\mathrm{fs}})}, \quad (15)$$

and the constant K_{fs} for triaxial extension becomes

$$K_{\mathrm{fs}} = \frac{3 + M_{\mathrm{fs}}}{3 - 2M_{\mathrm{fs}}} \quad (16)$$

Similarly, the critical state parameter for triaxial extension, M_{fs}, can be obtained from $M_{\mathrm{fs}} = 6\sin\phi'_{\mathrm{fs}}/(3 + \sin\phi'_{\mathrm{fs}})$.

Ignoring the difference between total and plastic strains, the flow rules (Eqs. 12 and 15) for fiber sand are plotted in terms of η and β, as depicted in Fig. 9 for $M_{\mathrm{fs}} = 1.4$ and $A = 0.1$. For comparison, Rowe's stress–dilatancy with $M_s = 1$ is also shown in Fig. 9. Evidently, the flow rules do not have the same shape for sand and sand fiber. The fiber sand will reach a higher stress ratio η than that of the pure sand with the same dilatancy angle β.

4.4 Stress–dilatancy relationship for fiber-reinforced sand under plane strain

For the conditions of plane strain, provided the principle axes of strain increment and axes of stress are coaxial for fiber soils, the stress dilatancy relationship, i.e., Eq. 4, becomes

$$\frac{\sigma'_1\delta\varepsilon_1}{-(\sigma_3 + \sigma_{\mathrm{FR}})\delta\varepsilon_3} = K_{\mathrm{fs}} \quad (17)$$

Since the intermediate principle stress does not contribute to the work, based on the Mohr circles of effective stresses and strain increments, we have

$$\frac{\sigma'_1}{\sigma'_3} = \frac{1 + \sin\phi'_m}{1 - \sin\phi'_m}, \quad \frac{-\delta\varepsilon'_1}{\delta\varepsilon'_3} = \frac{1 - \sin\psi}{1 + \sin\psi} \quad (18)$$

where ϕ'_m is the mobilized friction angle and ψ is the angle of dilation for fiber soil. At the critical state, we obtain

$$K_{\mathrm{fs}} = \frac{1 + \sin\phi'_{\mathrm{cs}}}{1 - \sin\phi'_{\mathrm{cs}}} \quad (19)$$

Eq. 17 can be rearranged as

$$\sin\phi'_m = \frac{2\sin\phi'_{\mathrm{cs}} + 2\sin\psi + A(1 + \sin\phi'_{\mathrm{cs}})(1 + \sin\psi)}{2 + 2\sin\phi'_{\mathrm{cs}}\sin\psi - A(1 + \sin\phi'_{\mathrm{cs}})(1 + \sin\psi)} \quad (20)$$

The influence of A on the stress–dilatancy relationships under plane strain conditions is plotted in Fig. 10. Figure 10 shows that the mobilized friction angle for fiber sand will be higher than that for the pure sand, with the same angle of dilation. If $A = 0$, $\phi_{\mathrm{fs}} = \phi$, the stress dilatancy will be same as Rowe's dilatancy relationship.

5 Comparisons between stress–dilatancy predictions and experimental data

5.1 Fiber-reinforced Nanjing sand

Table 3 shows the parameters for fiber-reinforced Nanjing sand. The presented stress–dilatancy relationship is calibrated using the triaxial compression tests for fiber-reinforced Nanjing sand with fiber content of $\chi_{\mathrm{w}} = 0.35\%$. Experimental data are plotted in the stress–dilatancy diagrams (Fig. 11). For comparison, the presented stress–dilatancy relationship (Eq. 12) and Rowe's original stress–dilatancy relationship were also plotted in the same figure. The addition of fibers caused the soil behavior to diverge

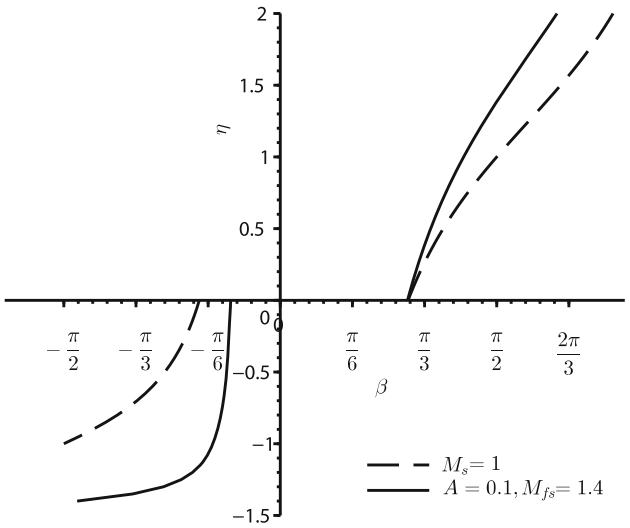

Fig. 9 Rowe's stress–dilatancy and the new presented stress–dilatancy relationships under CTC and CTE conditions

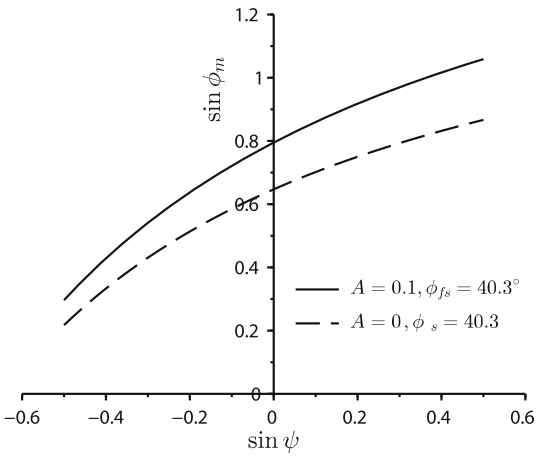

Fig. 10 Rowe's stress–dilatancy and the new presented stress–dilatancy relationships under plane strain conditions

Table 3 Parameters for fiber-reinforced Nanjing sand

Material	σ_r' (kPa)	ϕ	M
Sand	50, 100, 200, 300	$\phi = 31.1°$	$M = 1.25$
Sand fiber	50, 100	$\phi_{fs} = 40.3°$	$M_{fs} = 1.65$
Sand fiber	200, 300	$\phi_{fs} = 34.1°$	$M_{fs} = 1.38$

from the dilatancy trend from the pure sand. Although these values of β have been calculated from total strain increments, it is accepted that the stress–dilatancy relationship for fiber sand provides a reasonable description of the plastic flow of fiber-reinforced sand. The proposed stress–dilatancy relationship has met with the data better than Rowe's original stress–dilatancy relationship. The presented stress–dilatancy relationship generally reproduces the main dilatancy features of the behavior of reinforced Nanjing sand.

5.2 Fiber-reinforced Hostun RF sand

The Hostun RF sand reinforced with short polypropylene fibers has been tested by Diambra et al. [5] in conventional triaxial compression and extension. In Fig. 12, the stress–dilatancy relationship for the fiber sand composite was calibrated against the experimental results of drained triaxial compression and extension tests. The new presented stress–dilatancy relationship is represented by the thick line, whereas Rowe's original stress–dilatancy relationship is presented by dash line. The proposed stress–dilatancy relationship has met with the data better than Rowe's original stress–dilatancy relationship, which indicted that the proposed stress–dilatancy relationship provides a reasonable description of the plastic flow of fiber sand (Table 4).

6 Conclusions

The dilatancy characteristics and the stress–strain behavior of fiber sand are linked. This link was thought of as a description of the way in which energy is dissipated as a fiber sand specimen is sheared. From the experimental data and the stress–dilatancy relationship presented above, the stress–strain characteristics and dilatancy behavior for the fiber-reinforced sand can be drawn as follows:

1. Experiment data have been presented from conventional triaxial compression tests which were carried out to investigate the reinforcement of uniform distributed

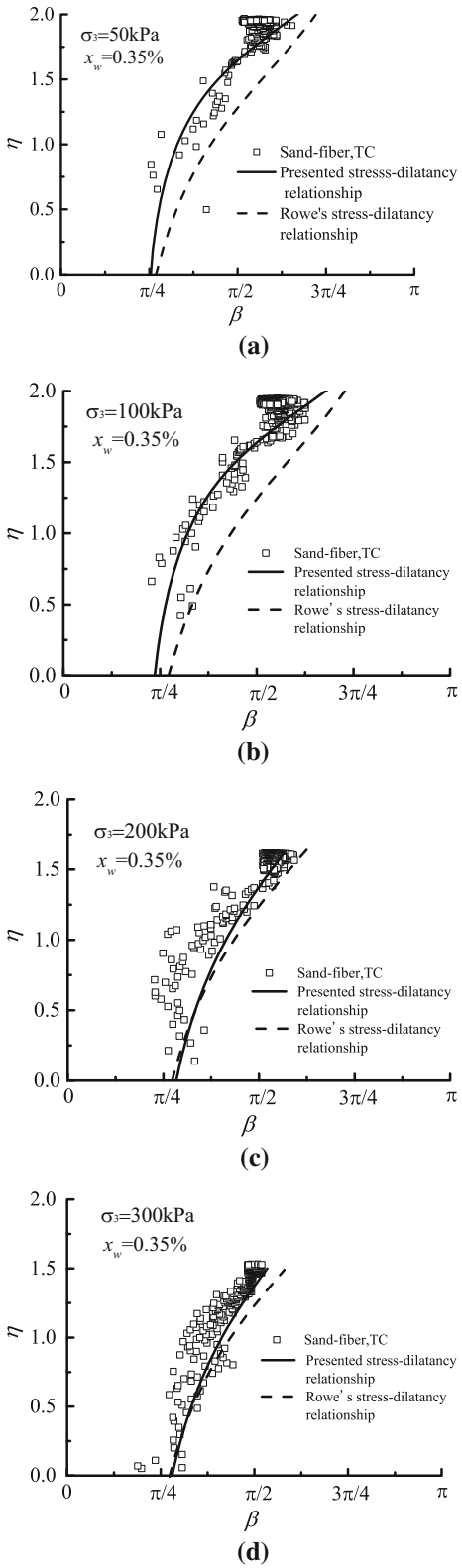

Fig. 11 Stress–dilatancy simulations for fiber-reinforced Nanjing sand with different confining pressures

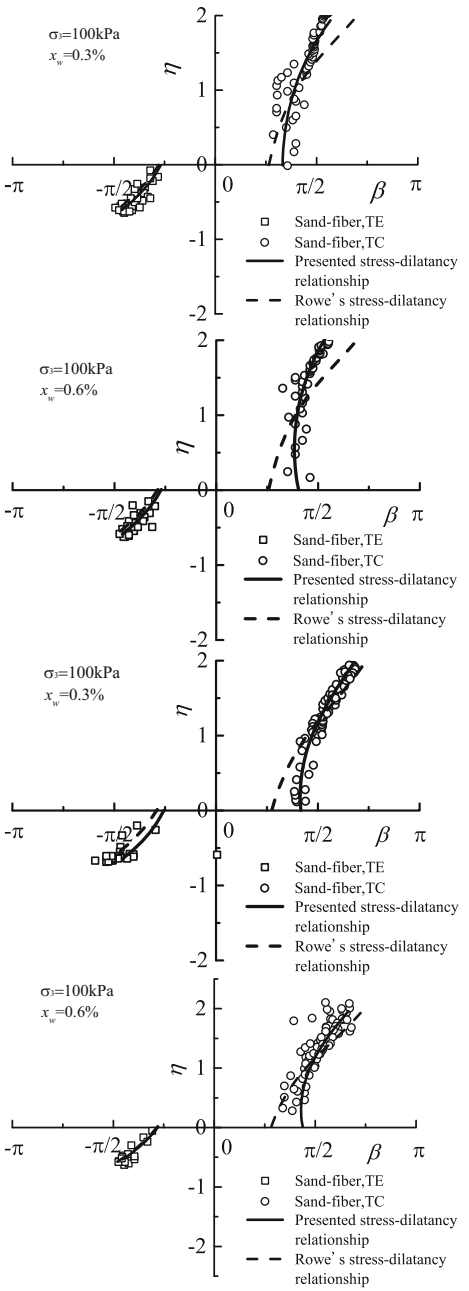

Fig. 12 Simulations for reinforced specimens at 100 kPa confining cell pressure Data adapted from Diambra et al. [5]

Table 4 Parameters for fiber-reinforced Hostun RF sand [5]

Materials	χ_w	e_c	ϕ (°)	M (TC)	M (TE)
Sand	0	0.991	33.5	1.42	0.62
Sand fiber	0.3%	0.966	36.2	1.64	0.62
Sand fiber	0.6%	0.945	38.5	1.76	0.62
Sand	0	0.833	33.1	1.16	0.63
Sand fiber	0.3%	0.816	34.5	1.23	0.67
Sand fiber	0.6%	0.798	36.9	1.25	0.60

fiber on the stress–strain–strength behavior of Nanjing sand.

2. Evaluation of the stress–strain–volumetric behavior of fiber-reinforced Nanjing sand with various fiber contents, χ_w, was proposed to account for the contribution of fiber-induced tension on soil strength.
3. The reinforcing effect of fiber on the effective confining stress was assessed in terms of σ_{FR}, which was provided by the tension mobilized by the fibers.
4. Accounting for the fiber reinforcement, a new stress–dilatancy relationship was proposed for fiber-reinforced sand based on Rowe's stress–dilatancy for granular materials. Model simulations show that the presented stress–dilation relationship predicts dilatancy of the fiber-reinforced sand better than that of the original Rowe's dilatancy.

Acknowledgements The authors would like to acknowledge the supports provided by the National Natural Science Foundation of China (No. 11402109) and the Natural Science Foundation of Jiangsu Province (No. BK20130909). The authors appreciate the comments made by the reviewer which help improve the quality of the manuscript. The authors would like to thank Dr. Dan Su, Dr. Zhu Song and Dr. Weiyun Chen for valuable comments and suggestions on the paper. Yuxia Kong thanks the China Scholarship Council for supporting her time in residence at RMIT University under visiting scholar award 201808320020.

References

1. Bolton M (1986) The strength and dilatancy of sands. Géotechnique 36(1):65–78
2. Consoli NC, Casagrande MDT, Coop MR (2007) Performance of a fibre-reinforced sand at large shear strains. Géotechnique 57(9):751–756
3. Diambra A, Ibraim E (2015) Fibre-reinforced sand: interaction at the fibre and grain scale. Géotechnique 65(4):296–308
4. Diambra A, Russell AR, Ibraim E, Wood DM (2007) Determination of fibre orientation distribution in reinforced sands. Géotechnique 57(7):623–628
5. Diambra A, Ibraim E, Wood DM, Russell A (2010) Fibre reinforced sands: experiments and modelling. Geotext Geomembr 28(3):238–250
6. Gray DH, Al-Refeai T (1986) Behavior of fabric-versus fiber-reinforced sand. J Geotech Eng 112(8):804–820
7. Heineck KS, Coop MR, Consoli NC (2005) Effect of microreinforcement of soils from very small to large shear strains. J Geotech Geoenviron Eng 131(8):1024–1033
8. Hendry MT, Sharma JS, Martin CD, Barbour SL (2012) Effect of fibre content and structure on anisotropic elastic stiffness and shear strength of peat. Can Geotech J 49(4):403–415
9. Houlsby G (1991) How the dilatancy of soils affects their behaviour. In: Proceedings of 10th European conference on soil mechanics and foundation engineering, Florence
10. Kruyt N, Rothenburg L (2016) A micromechanical study of dilatancy of granular materials. J Mech Phys Solids 95:411–427
11. Landva A, La Rochelle P (1983) Compressibility and shear characteristics of radforth peats. ASTM Spec Tech Publ 820:157–191

12. Li M, He H, Senetakis K (2017) Behavior of carbon fiber-reinforced recycled concrete aggregate. Geosynth Int 24(5):480–490
13. Madhusudhan BN, Baudet BA, Ferreira PMV, Sammonds P (2017) Performance of fiber reinforcement in completely decomposed granite. J Geotech Geoenviron Eng 143(8):04017038
14. Maher MH, Gray DH (1990) Static response of sands reinforced with randomly distributed fibers. J Geotech Eng 116(11):1661–1677
15. Maheshwari BK, Singh HP, Saran S (2012) Effects of reinforcement on liquefaction resistance of solani sand. J Geotech Geoenviron Eng 138(7):831–840
16. Reynolds O (1885) On the dilatancy of media composed of rigid particles in contact with experimental illustrations. Philos Mag Ser 5 20(127):469–481
17. Rifai SM, Miller CJ (2009) Theoretical assessment of increased tensile strength of fibrous soil undergoing desiccation. J Geotech Geoenviron Eng 135(12):1857–1862
18. Rowe PW (1962) The stress–dilatancy relation for static equilibrium of an assembly of particles in contact. Proc R Soc Lond A Math Phys Eng Sci 269(1339):500–527
19. Santos AD, Consoli N, Heineck K, Coop M (2010) High-pressure isotropic compression tests on fiber-reinforced cemented sand. J Geotech Geoenviron Eng 136(6):885–890
20. Santos APS, Consoli NC, Baudet BA (2010) The mechanics of fibre-reinforced sand. Géotechnique 60(10):791–799
21. Tang C, Shi B, Gao W, Chen F, Cai Y (2007) Strength and mechanical behavior of short polypropylene fiber reinforced and cement stabilized clayey soil. Geotext Geomembr 25(3):194–202
22. Tang CS, Shi B, Zhao LZ (2010) Interfacial shear strength of fiber reinforced soil. Geotext Geomembr 28(1):54–62
23. Wan RG, Guo PJ (2004) Stress dilatancy and fabric dependencies on sand behavior. J Eng Mech 130(6):635–645
24. Wood DM, Diambra A, Ibraim E (2016) Fibres and soils: a route towards modelling of root–soil systems. Soils Found 56(5):765–778
25. Zornberg JG (2002) Discrete framework for limit equilibrium analysis of fibre-reinforced soil. Géotechnique 52(8):593–604